Journal of Remote Sensing and GIS Applications in Environmental Sciences
rsgi.tabrizu.ac.ir

Spatio-Temporal Monitoring and Analysis of Water Surface Changes in Mahabad Dam Using an Integrated Data-Driven Approach Based on Sentinel-1 Data and Climatic Variables

Samaneh Bagheri[1], Sadra Karimzadeh[2]✉, Bakhtiar Feizizadeh[3] Saeed Samadianfard[4]

1. Ph.D Student, Department of remote sensing and GIS, Faculty of Planning and Environmental Sciences, University of Tabriz. Tabriz, Iran. E-mail: samanehbagheri99@gmail.com
2. Corresponding Author, Associate Professor. Department of remote sensing and GIS, Faculty of Planning and Environmental Sciences, University of Tabriz.Tabriz, Iran. E-mail: sadra.karimzadeh@gmail.com
3. Professor. Department of remote sensing and GIS, Faculty of Planning and Environmental Sciences, University of Tabriz.Tabriz, Iran. E-mail: bakhtiar.feizizadeh@gmail.com
4. Associate Professor. Department of Water Engineering, Faculty of Agriculture, University of Tabriz.Tabriz, Iran. E-mail: samaddianfard@gmail.com

Article Info

Article type:
Research Article

Article history:
Received: 2 September 2025
Revised: 6 December 2025
Accepted: 29 January 2026
Published: 29 April 2026

Keywords:
Mahabad Dam,
Sentinel-1,
XGBoost,
Support Vector Machine,
Water Surface Area.

ABSTRACT

Accurate monitoring of reservoir water surface area is essential for sustainable water resource management, particularly in arid and semi-arid regions where water availability is highly sensitive to climatic variability and anthropogenic pressures. Sentinel-1 synthetic aperture radar (SAR) data, with its all-weather and day-night imaging capability, provides a reliable framework for investigating surface water dynamics while overcoming the limitations of optical imagery. In this study, 360 monthly averaged ascending Sentinel-1 images acquired in VV and VH polarizations from January 2017 to December 2024 were processed to analyze the spatio-temporal variations in the water surface area of Mahabad Dam. Ascending orbit images were selected due to clearer reservoir boundary delineation, whereas descending images were excluded because of reduced visibility associated with acquisition geometry. Water body extraction was performed using a Support Vector Machine (SVM) classifier with a radial basis function (RBF) kernel. Prior to classification, a 3 × 3 Lee filter was applied to reduce speckle noise. The model was trained using 1,000 reference samples (500 water and 500 non-water), manually selected based on visual interpretation of SAR imagery and ancillary data. Classification accuracy was assessed monthly using Overall Accuracy (OA), User's Accuracy (UA), and the Kappa coefficient, ensuring the reliability of the extracted water surface area. To further enhance the analysis, the XGBoost machine learning model was employed to integrate SAR-derived water surface area with key climatic variables, including precipitation and temperature. The gradient boosting structure of XGBoost enabled effective modeling of complex, nonlinear relationships between climatic drivers and reservoir dynamics. Model evaluation indicated that Scenario 3 achieved the highest performance (RMSE = 0.526, MAE = 0.464, R^2 = 0.911, NSE = 0.911, WI = 0.977), while Scenario 4 showed the weakest performance. Overall, the results demonstrate that the synergistic integration of SAR remote sensing data and advanced machine learning techniques provides a robust, scalable, and efficient framework for monitoring and forecasting reservoir water surface area dynamics. This framework offers valuable insights for improving water resource management, supporting drought mitigation and adaptation strategies, and contributing to sustainable watershed planning in data-scarce and climate-sensitive regions. Nevertheless, the study is limited by its focus on a single reservoir and a restricted set of climatic variables. Future research should extend this approach by incorporating additional hydro-meteorological factors, exploring alternative machine learning models, and applying the framework to multiple reservoirs to enhance its generalizability.

Cite this article: Bagheri, S., Karimzadeh, S., Feizizadeh, B. & Samadianfard, S. (2026). Spatio-Temporal Monitoring and Analysis of Water Surface Changes in Mahabad Dam Using an Integrated Data-Driven Approach Based on Sentinel-1 Data and Climatic Variables. *Journal of Remote Sensing and GIS Applications in Environmental Sciences*, 6 (19), 90-108 http//doi.org/10.22034/rsgi.2026.71832.1157

Publisher: University of Tabriz.
DOI: http//doi.org/10.22034/rsgi.2026.71832.1157

Journal of Remote Sensing and GIS Applications in Environmental Sciences
rsgi.tabrizu.ac.ir

Introduction

Accurate monitoring of reservoir surface water area is a key requirement for sustainable water resources management, particularly in arid and semi-arid regions where water availability is strongly affected by climatic variability and increasing anthropogenic pressures. Conventional in-situ measurements are often limited by high costs, sparse spatial coverage, and data gaps. In this context, Synthetic Aperture Radar (SAR) data from the Sentinel-1 mission provide a reliable and continuous source of information for surface water monitoring due to their all-weather and day-and-night imaging capability. The main objective of this study is to assess the effectiveness of integrating Sentinel-1 SAR data with machine-learning techniques to extract and predict surface water area dynamics of the Mahabad Dam reservoir.

Data and Method

In this study, a total of 360 ascending Sentinel-1 SAR images with VV and VH polarizations acquired during the period 2017–2024 were processed. Standard preprocessing steps, including speckle noise reduction, radiometric calibration, and terrain correction, were applied prior to analysis. Surface water bodies were extracted using the Support Vector Machine (SVM) classification algorithm. The extracted surface water areas were then integrated with key climatic variables, including precipitation, air temperature, evaporation, and relative humidity. The Extreme Gradient Boosting (XGBoost) algorithm was employed to model and predict surface water area variations. Several modeling scenarios were designed using different combinations of input variables to evaluate the contribution of climatic factors. Model performance was assessed using statistical indicators such as RMSE, MAE, coefficient of determination (R^2), Nash–Sutcliffe efficiency (NSE), and Willmott's index (WI).

Results and Discussion

The results demonstrated that Sentinel-1 SAR data are highly capable of capturing seasonal and interannual variations in reservoir surface water area. The XGBoost model showed strong predictive performance across all scenarios. Among the tested scenarios, Scenario 3 achieved the best performance, yielding the lowest error values and the highest agreement between predicted and observed surface water areas. This finding highlights evaporation as a dominant climatic driver controlling surface water area fluctuations in the reservoir. In contrast, scenarios relying solely on precipitation exhibited weaker performance, indicating that precipitation alone is insufficient to explain surface water dynamics in arid environments. These results emphasize the importance of considering combined climatic effects when modeling reservoir behavior.

Conclusion

Overall, this study demonstrates that the integration of Sentinel-1 SAR data with advanced machine-learning algorithms, particularly XGBoost, provides an efficient, robust, and scalable framework for monitoring and predicting reservoir surface water area dynamics. The proposed approach offers valuable insights for reservoir operation, drought mitigation, and sustainable water resources management, especially in data-scarce regions. The methodology can be readily transferred to other reservoirs with similar hydro-climatic conditions, supporting informed decision-making under increasing climate variability.

References

Ahmad, S.K., Hossain, F., Eldardiry, H. and Pavelsky, T.M., (2019). A fusion approach for water area classification using visible, near infrared and synthetic aperture radar for South Asian conditions. *IEEE Transactions on Geoscience and Remote Sensing*, 58(4), pp.2471-2480.

Bagheri, S., Karimzadeh, S., Feizizadeh, B., & Samadianfard, S. (2025). *An integrated data-driven approach using dual polarized SAR data for spatiotemporal analysis of water surface changes*. Advances in Space Research. Advance online publication.

Bao, L., Lv, X. and Yao, J., (2021). Water extraction in SAR images using features analysis and dual-threshold graph cut model. *Remote Sensing*, 13(17), p.3465.

Bolanos, S., Stiff, D., Brisco, B. and Pietroniro, A., (2016). Operational surface water detection and monitoring using Radarsat 2. *Remote Sensing*, 8(4), p.285.

Brisco, B., (2015). *Mapping and monitoring surface water and wetlands with synthetic aperture radar*. Remote Sensing of Wetlands: Applications and Advances, pp.119-136.

Cohen, J., (1960). A coefficient of agreement for nominal scales. *Educational and psychological measurement*, 20(1), pp.37-46.

Congalton, R.G. and Green, K., (2019). *Assessing the accuracy of remotely sensed data: principles and practices*. CRC press.

Crétaux, J.F., Abarca-del-Río, R., Berge-Nguyen, M., Arsen, A., Drolon, V., Clos, G. and Maisongrande, P., (2016). Lake volume monitoring from space. *Surveys in Geophysics*, 37(2), pp.269-305.

Foody, G.M. and Mathur, A., (2004). A relative evaluation of multiclass image classification by support vector machines. *IEEE Transactions on geoscience and remote sensing*, 42(6), pp.1335-1343.

Goumehei, E., Tolpekin, V., Stein, A. and Yan, W., (2019). Surface water body detection in polarimetric SAR data using contextual complex Wishart classification. *Water Resources Research*, 55(8), pp.7047-7059.

Guo, Z., Wu, L., Huang, Y., Guo, Z., Zhao, J. and Li, N., (2022). Water-body segmentation for SAR images: past, current, and future. *Remote Sensing*, 14(7), p.1752.

Hong, S., Jang, H., Kim, N. and Sohn, H.G., (2015). Water area extraction using RADARSAT SAR imagery combined with landsat imagery and terrain information. *Sensors*, 15(3), pp.6652-6667.

Kreiser, Z., Killough, B. and Rizvi, S.R., (2018, July). *Water across synthetic aperture radar data (wasard): Sar water body classification for the open data cube*. In IGARSS 2018-2018 IEEE International Geoscience and Remote Sensing Symposium (pp. 437-440). IEEE.

Li, J. and Wang, S., 2015. An automatic method for mapping inland surface waterbodies with Radarsat-2 imagery. *International Journal of Remote Sensing*, 36(5), pp.1367-1384.

Li, M., Hong, L., Guo, J. and Zhu, A., (2022). Automated extraction of lake water bodies in complex geographical environments by fusing Sentinel-1/2 Data. *Water*, 14(1), p.30.

Liang, J. and Liu, D., (2020). A local thresholding approach to flood water delineation using Sentinel-1 SAR imagery. ISPRS *journal of photogrammetry and remote sensing*, 159, pp.53-62.

Lv, W., Yu, Q. and Yu, W., (2010, October). *Water extraction in SAR images using GLCM and support vector machine*. In IEEE 10th international conference on signal processing proceedings.

Matgen, P., Hostache, R., Schumann, G., Pfister, L., Hoffmann, L. and Savenije, H.H.G., (2011). Towards an automated SAR-based flood monitoring system: Lessons learned from two case studies. *Physics and Chemistry of the Earth*, Parts A/B/C, 36(7-8), pp.241-252.

McFeeters, S.K., (1996). The use of the Normalized Difference Water Index (NDWI) in the delineation of open water features. *International journal of remote sensing*, 17(7), pp.1425-1432.

Medina, C.E., Gomez-Enri, J., Alonso, J.J. and Villares, P., 2008. Water level fluctuations derived from ENVISAT Radar Altimeter (RA-2) and in-situ measurements in a subtropical waterbody: Lake Izabal (Guatemala). *Remote Sensing of Environment*, 112(9), pp.3604-3617.

Morandeira, N.S., Grings, F., Facchinetti, C. and Kandus, P., 2016. Mapping plant functional types in floodplain wetlands: an analysis of C-band polarimetric SAR data from RADARSAT-2. *Remote Sensing*, 8(3), p.174.

Mountrakis, G., Im, J. and Ogole, C., (2011). Support vector machines in remote sensing: A review. *ISPRS journal of photogrammetry and remote sensing*, 66(3), pp.247-259.

Qin, X., Yang, J., Li, P. and Sun, W., (2019, July). *Research on water body extraction from Gaofen-3 imagery based on polarimetric decomposition and machine learning*. In IGARSS 2019-2019 IEEE International Geoscience and Remote Sensing Symposium (pp. 6903-6906). IEEE.

Rajendiran, N. and Kumar, L.S., (2023). Pixel level feature extraction and machine learning classification for water body extraction. *Arabian Journal for Science and Engineering*, 48(8), pp.9905-9928.

Santoro, M., Wegmüller, U., Lamarche, C., Bontemps, S., Defourny, P. and Arino, O., (2015). Strengths and weaknesses of multi-year Envisat ASAR backscatter measurements to map permanent open water bodies at global scale. *Remote Sensing of Environment*, 171, pp.185-201.

Schölkopf, B. and Smola, A.J., (2002). *Learning with kernels: support vector machines, regularization, optimization, and beyond*. MIT press.

Stehman, S.V., 1997. Selecting and interpreting measures of thematic classification accuracy. *Remote sensing of Environment*, 62(1), pp.77-89.

Weekley, D. and Li, X., (2019). Tracking multidecadal lake water dynamics with Landsat imagery and topography/bathymetry. *Water Resources Research*, 55(11), pp.8350-8367.

Wu, L., Wang, L., Min, L., Hou, W., Guo, Z., Zhao, J. and Li, N., (2018). Discrimination of algal-bloom using spaceborne SAR observations of Great Lakes in China. *Remote Sensing*, 10(5), p.767.

Xu, H., 2006. Modification of normalised difference water index (NDWI) to enhance open water features in remotely sensed imagery. *International journal of remote sensing*, 27(14), pp.3025-3033.

Yang, S., Wang, L., Yuan, Y., Fan, L., Wu, Y., Sun, W. and Yang, G., (2024). Recognition of small water bodies under complex terrain based on SAR and optical image fusion algorithm. *Science of The Total Environment*, 946, p.174329.

Zhang, P., Chen, L., Li, Z., Xing, J., Xing, X. and Yuan, Z., 2019. Automatic extraction of water and shadow from SAR images based on a multi-resolution dense encoder and decoder network. *Sensors*, 19(16), p.3576.

Zhou, Y.N., Luo, J., Shen, Z., Hu, X. and Yang, H., 2014. Multiscale water body extraction in urban environments from satellite images. I*EEE Journal of selected topics in applied earth observations and remote sensing*, 7(10), pp.4301-4312.

Introduction

Surface water bodies such as lakes and reservoirs are critical components of hydrological systems and play an essential role in water resource management, ecological sustainability, and socioeconomic development. However, climate change and increasing human activities have significantly altered their spatial extent and temporal dynamics, emphasizing the need for continuous and reliable monitoring (Zhang et al., 2019a, b; Guo et al., 2022). Lakes and reservoirs are also recognized as sensitive indicators of global climate variability, and their surface fluctuations provide valuable insight into regional water balance processes (Crétaux et al., 2016). In many regions, in situ observations are sparse or unavailable due to logistical constraints, political limitations, or the remoteness of water bodies, making satellite-based monitoring indispensable (Medina et al., 2008).

Remote sensing has been widely adopted for surface water mapping and monitoring. Optical imagery offers high spatial resolution and multispectral information that enables intuitive interpretation of surface features; however, its effectiveness is limited by cloud cover, atmospheric effects, and illumination conditions (Zhou et al., 2014; Ahmad et al., 2019; Yang et al., 2024). Numerous studies have demonstrated the effectiveness of spectral water indices derived from optical sensors, such as Landsat and Sentinel-2, for delineating surface water bodies and supporting water resource management, particularly in lake environments (Asghari-Sarascanrud et al., 2024). Nevertheless, optical-based approaches remain sensitive to atmospheric conditions, turbid water, and complex land–water boundaries, which often result in misclassification and reduced accuracy.

To address these limitations, Synthetic Aperture Radar (SAR) data have been increasingly utilized due to their all-weather, day-and-night imaging capability, allowing consistent observation of water surfaces under diverse environmental conditions (Goumehei et al., 2019; Weekley and Li, 2019). SAR imagery has proven particularly valuable for flood and drought monitoring, supporting timely decision-making in water management and disaster response (Bao et al., 2021). SAR-based water extraction methods have traditionally relied on thresholding techniques that exploit the low backscatter characteristics of open water, including histogram-based thresholding, Otsu's method, and statistical distribution models (Santoro et al., 2015; Li and Wang, 2015; Matgen et al., 2011; Liang and Liu, 2020; Hong et al., 2015; Bolanos et al., 2016). To enhance classification accuracy, these approaches have been combined with supervised classification, segmentation, and machine learning algorithms (Brisco, 2015; Qin et al., 2019).

Among machine learning classifiers, the Support Vector Machine (SVM) has demonstrated robust performance in SAR-based water body extraction, particularly when incorporating polarization information and textural features (Lv et al., 2010; Kreiser et al., 2018; Wu et al., 2018). Beyond water surface mapping, SAR-based interferometric techniques have also been extensively applied to investigate surface deformation and subsidence phenomena. For example, recent studies have integrated Sentinel-1 D-InSAR products with spatial statistical models, such as Ordinary Least Squares (OLS), to analyze the driving factors of land subsidence, highlighting the dominant role of groundwater level decline and land-use change in urban environments (Norouzi-Moghadam et al., 2022).

SAR interferometry has further been employed to assess deformation in large hydraulic infrastructures. Using SBAS-InSAR and ALOS-2 PALSAR-2 data, Karimzadeh et al. (2025) analyzed surface subsidence at the Mosul Dam in Iraq, demonstrating the capability of multi-temporal InSAR techniques to detect millimeter-scale deformation and provide valuable insights into the structural behavior of large dams. These studies underscore the importance of advanced SAR-based methods for monitoring water-related systems and associated hazards in arid and semi-arid regions.

Recent research has increasingly focused on integrating SAR-derived water surface information with machine learning techniques to analyze and predict reservoir dynamics. In this context, Bagheri et al. investigated reservoir water surface variations using Sentinel-1 SAR imagery and machine

learning models at the Boukan embankment dam in western Iran, demonstrating that radar-based approaches can accurately capture temporal surface water changes and outperform conventional optical index-based methods.

Despite these advances, most previous studies have focused on short-term analyses or single-variable evaluations, providing limited insight into the combined impact of climatic factors on reservoir water dynamics. In particular, long-term spatio-temporal assessments using dual-polarized Sentinel-1 SAR data integrated with multiple climatic variables remain scarce, especially in semi-arid regions of the Middle East where reservoirs play a crucial role in water supply and drought resilience.

This study addresses this gap by developing an integrated data-driven framework that combines multi-year (2017–2024) dual-polarized Sentinel-1 imagery with key climatic variables to monitor and predict water surface dynamics in the Mahabad Dam. The novelty of this research lies in (i) the use of an extensive multi-year SAR dataset for continuous monitoring, (ii) the integration of SAR-derived water surface information with climatic predictors through machine learning (XGBoost) modeling, and (iii) the comprehensive assessment of the relative influence of individual climatic variables on reservoir surface fluctuations.

The proposed framework offers a robust and scalable approach for long-term reservoir monitoring and prediction in data-scarce, semi-arid environments, providing new insights into the climate-driven dynamics of surface water systems.

Study area and dataset

- **Study area**

The Mahabad Dam is an embankment clay-core dam located in northwestern Iran and plays key roles in regional water supply, irrigation, and hydroelectric power generation. The dam has a normal reservoir capacity of 196.7 million cubic meters, a crest length of 700 meters, and a height of 45 meters measured from the riverbed(www.sceg.ir).

Seasonal reservoir conditions at the Mahabad Dam between 2017 and 2024 were examined using Sentinel-1 SAR observations. The dataset includes quarterly representations for each year, organized with years from 2017 to 2024 and the four seasonal periods (winter, spring, summer, and autumn). These seasonal snapshots provide an overview of the general hydrological variability of the reservoir throughout the year.

Overall, the reservoir typically shows larger surface extents during the wet season (winter–spring) and comparatively smaller extents during the drier months (summer–autumn), reflecting the broader climatic characteristics of the region. These patterns are described in detail and quantitatively analyzed in the Results section of the manuscript.

Understanding these seasonal water surface variations is important for water-resources planning, including drinking-water management and irrigation scheduling. The geographical location of the study area is presented in Figure 1.

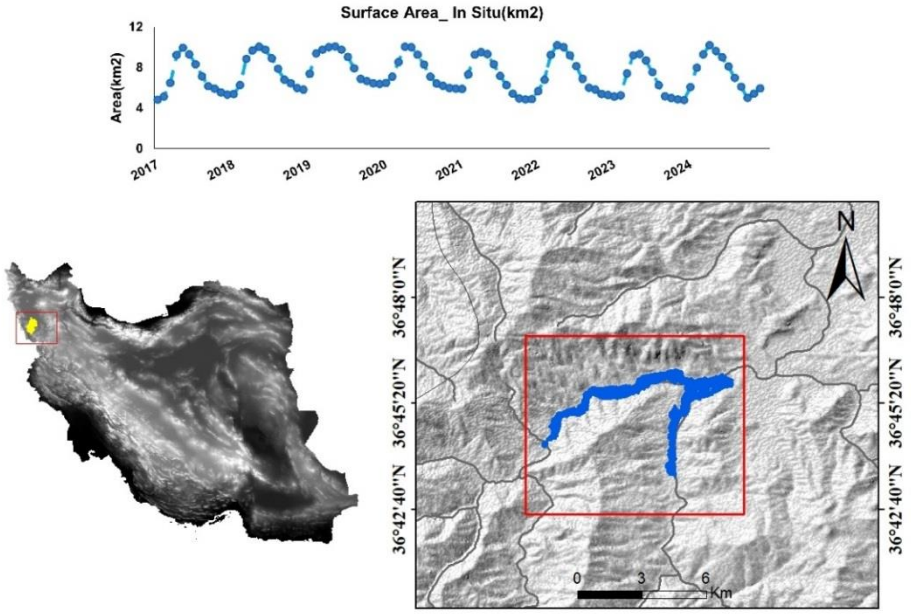

Figure 1. study area

- **Dataset**

In this study, spatio-temporal monitoring of water surface changes in the Mahabad Dam reservoir was conducted using Sentinel-1 C-band SAR data spanning from January 2017 to December 2024. Monthly averaged images acquired in Interferometric Wide (IW) mode with a ground resolution of approximately 10 m were obtained exclusively from the ascending orbit, as this acquisition geometry provided clearer delineation of the reservoir boundary compared to descending passes.

All Sentinel-1 scenes were subjected to a standard preprocessing workflow to ensure radiometric consistency and spatial accuracy. This workflow included radiometric calibration to sigma-naught backscatter coefficients, speckle noise reduction using the Lee filter with a 3×3 window, and terrain correction based on the Shuttle Radar Topography Mission (SRTM) digital elevation model. These steps were applied uniformly to both VV and VH polarizations.

To enable meaningful comparison between polarizations and across acquisition dates, a min–max normalization was applied to the backscatter values. Specifically, VV and VH backscatter coefficients were normalized independently for each scene to a 0–1 range. Scene-wise normalization was selected to minimize the influence of temporal variations in imaging conditions and to preserve relative contrast within each acquisition.

Water surface extraction was conducted using a supervised classification approach, in which VV and VH polarizations were incorporated as two separate input features. No averaging, ratio, or composite index was derived from the dual-polarization data. Instead, both normalized VV and VH layers were directly supplied to the classifier to exploit their complementary sensitivity to surface roughness and dielectric properties.

A Support Vector Machine (SVM) classifier with a radial basis function (RBF) kernel was employed to discriminate between water and non-water classes. The model was trained using 1,000 manually selected samples, consisting of 500 water and 500 non-water pixels, distributed across the study area to capture spatial variability. Classification and accuracy assessment were performed on a monthly basis, and performance was evaluated using Overall Accuracy (OA), User's Accuracy (UA), and the Kappa coefficient.

The extracted monthly water surface extents were subsequently used for spatio-temporal analysis and integration with climatic variables in the subsequent modeling framework.

Methodological framework

The present study was conducted through three main stages, forming an integrated methodological framework for monitoring and predicting reservoir water surface area variations using SAR remote sensing data and advanced machine learning techniques. An overview of the proposed framework is presented in Figure 2.

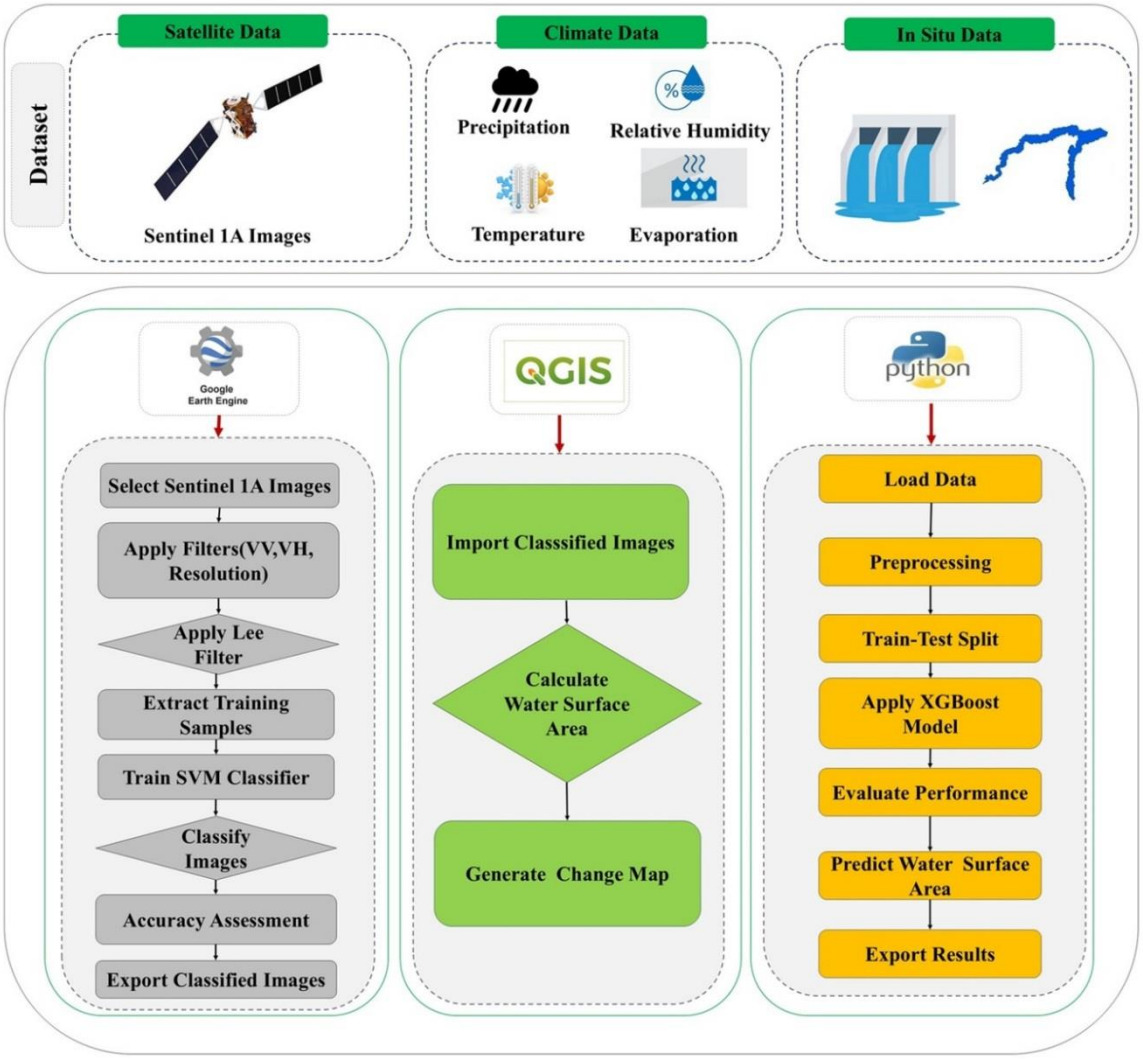

Figure 2. Methodology flowchart adopted in this study

- **Data Collection and Preprocessing**

In the first stage, comprehensive data acquisition and preprocessing were performed. A total of 360 ascending Sentinel 1 SAR images with consistent acquisition geometry were collected in VV and VH polarizations, fully covering the Mahabad Dam reservoir within the mid swath region. Owing to the all weather and day night imaging capability of Sentinel 1, these data provide a reliable basis for continuous reservoir monitoring under varying atmospheric conditions.

Initial preprocessing of Sentinel 1 imagery, including radiometric calibration and geometric correction, was conducted within the Google Earth Engine (GEE) platform. Geometric correction was implemented using the Range Doppler Terrain Correction method, which compensates for terrain induced distortions and sensor viewing geometry, ensuring accurate georeferencing of the imagery. Radiometric calibration was applied to normalize backscatter values and enable temporal consistency across the dataset. To further improve image quality, speckle noise reduction was applied using

adaptive filters, such as the Lee filter, within GEE. These additional preprocessing steps enhanced the clarity of water boundaries and improved the reliability of subsequent analyses.

Climatic data, including evaporation (E), temperature (T), precipitation (P), and relative humidity (RH), were obtained from the Iranian Meteorological Organization and the Iran Water Resources Management Company. Evaporation data correspond to measured pan evaporation recorded at nearby synoptic meteorological stations and were used directly without conversion to evapotranspiration.

The selected synoptic stations are located within and around the Mahabad reservoir basin. Considering the limited spatial extent of the basin and the relatively homogeneous semi-arid climatic conditions of the region, the recorded observations were considered representative of the basin-scale climatic variability.

Radiometric calibration was performed to convert the SAR backscatter to sigma-naught (σ^0). Speckle noise was reduced using a Lee filter with a 3 × 3 moving window. Terrain correction was carried out using the Range-Doppler Terrain Correction (RTC) method based on the SRTM digital elevation model with 30 m spatial resolution, which also accounts for variations in local incidence angle.

Following preprocessing, the VV and VH backscatter intensities were normalized independently using Min–Max scaling to the range [0,1]. This normalization was applied on a scene-wise basis to reduce inter-scene radiometric variability.

- **Water Surface Extraction and Machine Learning Integration**

In the second stage, water surface area extraction and data integration were carried out. The Support Vector Machine (SVM) classifier was employed to delineate water and non water classes from the preprocessed SAR images. SVM was selected due to its strong performance in high dimensional feature spaces and its robustness in binary classification problems involving SAR backscatter characteristics.

Following classification, the extracted water surface area information was integrated with climatic variables using the Extreme Gradient Boosting (XGBoost) model. XGBoost was chosen for its ability to handle nonlinear relationships, manage multicollinearity among input variables, and prevent overfitting through regularization. The model was implemented in a Python environment, where data normalization was performed using the StandardScaler function from the scikit learn library. Model training, hyperparameter tuning, and performance evaluation were conducted using standard error metrics, including root mean square error (RMSE), mean absolute error (MAE), coefficient of determination (R^2), Nash–Sutcliffe efficiency (NSE), and the Willmott Index (WI). Core Python libraries such as pandas, numpy, scikit learn, and XGBoost were utilized for data handling and model development.

The normalized VV and VH backscatter values were used directly as input features to the SVM classifier. No polarization ratios, band combinations, or texture features were derived, ensuring a parsimonious and reproducible feature set.

- **Validation, Analysis, and Visualization**

In the final stage, model validation and application were performed. Validation was conducted on a monthly basis by directly comparing the predicted water surface area values derived from SAR-based classification and XGBoost modeling with in situ measurements of the reservoir water surface area, which served as an independent reference dataset. Random data splitting was not applied, as preserving the temporal structure of the time-series data was essential for reliable validation. The strong agreement between observed and predicted values confirms the robustness and reliability of the proposed methodology.

Subsequently, the validated model was used to analyze seasonal patterns and spatio-temporal trends in reservoir water surface area, as well as to assess potential future changes under varying climatic conditions. Post-processing and spatial analysis were performed using QGIS, where tools

such as the Field Calculator, Zonal Statistics, and Print Layout were employed to compute water surface area statistics and generate high-quality maps illustrating temporal and spatial variations of the reservoir throughout the study period.

Water surface classification

Support Vector Machine (SVM) is a well-established kernel-based learning algorithm that has been extensively applied in remote sensing and image classification studies. Originally developed by Vapnik and colleagues in the late 1970s, SVM has demonstrated strong performance in discriminating complex land cover classes, particularly when dealing with high-dimensional datasets (Mountrakis et al., 2011). In its simplest formulation, SVM functions as a linear binary classifier by defining a separating hyperplane between two classes. This approach assumes that the input data are linearly separable within the original feature space.

When linear separability cannot be achieved, SVM overcomes this limitation by employing kernel functions that project the input data into a higher-dimensional feature space, enabling the construction of nonlinear decision boundaries. The optimal hyperplane is determined by maximizing the margin between classes, which is defined by a limited number of critical training samples known as support vectors (Schölkopf and Smola, 2002; Foody and Mathur, 2004). This margin-maximization property makes SVM particularly effective for binary classification tasks such as water and non-water separation in SAR imagery.

In the present study, SVM was applied to classify and extract the water surface area of the dam using paired VV and VH polarization Sentinel-1 SAR data. The classification procedure was implemented through a user-defined SVM algorithm developed within the Google Earth Engine (GEE) platform. GEE, as a cloud-based geospatial analysis environment, provides direct access to extensive satellite archives and computational resources, facilitating efficient large-scale processing. While Sentinel-1 data acquisition and preprocessing were handled through GEE's built-in functions, the water surface classification was performed by executing the custom SVM script designed by the authors within this platform (Table 1).

Table 1. Sentinel-1 data specifications

Satellite platform	**Sentinel-1A**
Frequency	5.405 GHz (C-band)
Product type	Ground Range Detected (GRD)
Sensor mode	Interferometric Wide Swath (IW)
Sub-swath	IW1
Polarization	Dual (VV and VH)
Pass direction	Ascending
Spatial resolution	20.4 m × 22.5 m (range × azimuth)
Incidence angle	angle 32.9◦
Swath width	251.8 km
Temporal resolution	12 day

Water surface prediction

In this study, observed water surface area records provided by the Iranian Water Resources Management Organization were utilized both to validate the accuracy of the water surface area extracted from SAR imagery and to support predictive modeling. The water surface area derived from the SVM classification results was integrated with climatic variables to investigate and forecast temporal variations in reservoir water extent. To achieve this objective, a set of eleven predictive scenarios was designed, each incorporating different combinations of input variables. A summary of the input parameters used in each scenario is presented in Table 2.

Climatic variables, including air temperature (T), relative humidity (RH), evaporation (E), and

precipitation (P), were combined with the SVM-derived water surface area as explanatory features for model development. This multi-source data integration approach was adopted to capture the combined influence of hydro-climatic conditions and observed reservoir dynamics on water surface area fluctuations, thereby improving the robustness and reliability of the predictive framework.

- **XGBoost Algorithm**

Extreme Gradient Boosting (XGBoost) is an advanced ensemble machine learning algorithm based on the gradient boosting framework, widely recognized for its high predictive accuracy and computational efficiency. XGBoost constructs a sequence of decision trees, where each successive tree is trained to minimize the residual errors of the previous ones. By employing both first- and second-order gradient information, the algorithm effectively captures complex nonlinear relationships between input variables and the target output.

One of the key advantages of XGBoost is its built-in regularization mechanism, which controls model complexity and reduces the risk of overfitting. Additionally, the algorithm efficiently handles multicollinearity among input features and can manage missing or noisy data, making it particularly suitable for environmental and hydrological applications. In this study, XGBoost was used to model the relationship between climatic variables and the observed water surface area of the reservoir.

Model training and evaluation were performed in a Python environment. Prior to modeling, all input variables were normalized to ensure consistency and improve convergence. Hyperparameters such as the number of trees, learning rate, maximum tree depth, and subsampling ratio were optimized through iterative tuning to achieve optimal model performance. The predictive capability of the model was assessed using multiple statistical metrics, including RMSE, MAE, R^2, Nash–Sutcliffe efficiency (NSE), and the Willmott Index (WI), allowing for a comprehensive evaluation of model accuracy across the different scenarios.

Table 2. Combinations of input variables across different scenarios (T (Monthly Average Temperature), RH (Monthly Average Relative Humidity), E (Total Monthly Evaporation), P (Total Monthly Precipitation)).

Scenarios	Input variables					
1	SVM	T				
2	SVM	RH				
3	SVM	E				
4	SVM	P				
5	SVM	E	T			
6	SVM	E	RH			
7	SVM	E	P			
8	SVM	E	P	T		
9	SVM	E	P	RH		
10	SVM	E	P	RH		T

Accuracy assessment

Accuracy assessment represents a fundamental step in remote sensing-based mapping to ensure the reliability of classification outputs. The predictive performance of the proposed approach was supported by a strong agreement between the SAR-derived results and in-situ observations, with correlation coefficients of 0.99 for VV and 0.98 for VH polarizations, indicating its suitability for continuous monitoring applications.

To evaluate the reliability of the water surface classification produced by the SVM algorithm implemented in the Google Earth Engine environment, several standard accuracy metrics were employed. These included overall accuracy (OA), the Kappa coefficient, producer's accuracy, and user's accuracy. Overall accuracy provides an aggregated measure of classification performance by

quantifying the proportion of correctly classified samples relative to the total number of reference observations. In other words, OA reflects the level of agreement between the classified map and ground truth data. The mathematical expression used to compute overall accuracy is presented below (Congalton and Green, 2019):

$$OA = \frac{\sum_{i=1}^{N} TP_i}{\sum_{i=1}^{N}(TP_i + FN_i + FP_i + TN_i)} \quad (1)$$

Where:

TP_i = True positive pixels in class *i*

FN_i= False negative pixels in class *i*

FP_i = False positive pixels in class *i*

TN_i= True negative pixels in class *i*

The Kappa coefficient is a statistical indicator used to quantify the level of agreement between classified results and reference data while correcting for agreement that may occur purely by chance. This metric provides insight into the extent to which the classification performance exceeds what would be expected from a random assignment of classes. The mathematical formulation of the Kappa coefficient is expressed as follows (Cohen, 1960):

$$\mathcal{K} = \frac{P_O - P_e}{1 - P_e} \quad (2)$$

Where:

P_O = Observed accuracy (Overall Accuracy)

P_e = Expected accuracy (chance agreement)

Producer's accuracy quantifies the proportion of reference samples for a given class that are correctly identified in the classified map. From the standpoint of ground truth data, this metric reflects how effectively the classification process captures each class. The corresponding formula used to calculate producer's accuracy is presented below (Stehman, 1997):

$$PA_i = \frac{TP_i}{TP_i + FN_i} \quad (3)$$

Where:

TP_i = True positive pixels in class *i*

FN_i= False negative pixels in class *i*

Producer's accuracy expresses the fraction of ground-reference samples belonging to a specific class that are accurately labeled in the classified output. Viewed from the reference data perspective, this measure indicates the ability of the classification method to correctly detect each class. The mathematical expression for computing producer's accuracy is provided below (Stehman, 1997):

$$UA_i = \frac{TP_i}{TP_i + FP_i} \quad (4)$$

Where:

TP_i= True positive pixels in class *i*

FP_i = False positive pixels in class *i*

Results

- **Results of image classification**

The spatial and temporal distribution of the dam's water surface area derived from Sentinel-1 SAR imagery highlights pronounced seasonal variability throughout the study period (Figures 3 and 4). The largest water surface extent is generally observed during spring, primarily due to increased precipitation and snowmelt contributions from upstream catchments, leading to a clear expansion of the reservoir boundary. In contrast, the minimum surface area typically occurs in autumn, reflecting reduced rainfall and cumulative evaporation losses following the summer season. Summer and winter represent transitional conditions, with summer showing gradual water surface contraction driven by high evaporation, while winter maintains relatively stable but lower extents compared to spring.

Figures 3 and 4 show the monthly water surface maps extracted using the SVM classifier from Sentinel-1 SAR imagery in VH and VV polarizations, respectively. While both polarizations successfully capture the seasonal dynamics of the reservoir, the VV polarization provides a clearer and more consistent delineation of water boundaries, particularly during low-water periods. This superiority can be attributed to the dominance of surface (Bragg) scattering from calm water surfaces in VV polarization, which results in lower and more stable backscatter values over water bodies. In contrast, VH polarization is more sensitive to volume scattering from surrounding vegetation and exposed shallow areas, leading to increased signal variability and reduced boundary clarity. Consequently, VV polarization demonstrates higher physical sensitivity and suitability for monitoring water surface fluctuations in the study area.

Figure 5 shows the temporal variations of the reservoir water surface area derived from Sentinel-1 SAR data using VV and VH polarizations compared with in-situ observations during the study period. The results demonstrate strong agreement between satellite-derived estimates and observed data, indicating that both polarizations successfully capture the seasonal fluctuations of reservoir water extent. Minor discrepancies are observed during certain periods; however, the overall temporal pattern and peak-to-low dynamics are well preserved. Overall, the consistency between satellite-derived results and field measurements confirms the robustness of the SVM-based water surface classification framework.

The temporal behavior of climatic variables, including precipitation, air temperature, relative humidity, and evaporation from 2017 to 2024, exhibits clear seasonal and interannual variability that directly influences reservoir dynamics (Table 3). The classification accuracy of the SVM model using VV and VH polarizations is evaluated in Figure 6 through multiple accuracy metrics, including overall accuracy (OA), kappa coefficient, producer's accuracy (PA), and user's accuracy (UA). The results indicate consistently high classification performance across the study period for both polarizations, with VV generally exhibiting slightly higher accuracy than VH. The high OA and kappa values confirm the reliability and robustness of the SVM-based water surface classification, while the balanced PA and UA values demonstrate stable discrimination between water and non-water classes.

In addition to qualitative temporal agreement, statistical analysis confirms the strength of these relationships. As presented in Figure 7, scatter plots between SAR-derived water surface areas and in-situ observations show strong linear associations, with coefficients of determination (R^2) of 0.963 for VV polarization and 0.916 for VH polarization. These correspond to Pearson correlation coefficients of approximately 0.98 and 0.96, respectively, indicating that the observed agreement is supported by robust statistical evidence rather than visual interpretation alone.

In addition to climatic influences, anthropogenic factors such as reservoir operation policies, irrigation demands, and land-use changes within the watershed may also affect water surface variability. Although these factors were not explicitly quantified in this study, their potential role in modulating observed trends should be considered in future research.

Accuracy metrics were computed for all months during the study period. For clarity and brevity, only the best- and worst-performing months together with the multi-year mean are summarized in Table 4. The SVM-VH classification achieved a maximum OA and Kappa of 1.00 during several spring and early summer months, while the lowest performance occurred in winter months (minimum

OA ≈ 0.82, Kappa ≈ 0.63). The relatively narrow range between extreme values and the high multi-year mean accuracy (OA ≈ 0.95, Kappa ≈ 0.90) indicate good temporal stability of the model. Similarly, the SVM-VV results exhibit slightly higher and more consistent performance, with a multi-year mean OA of approximately 0.97 and Kappa of 0.94, confirming the superior robustness of VV polarization for long-term reservoir water surface monitoring.

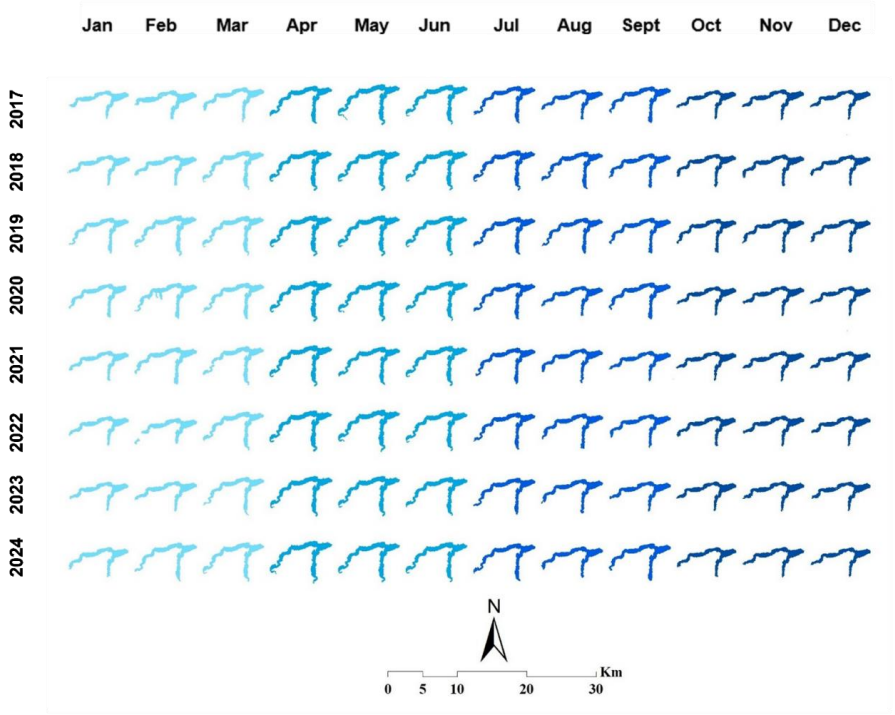

Figure 3. Changes in the water surface area of Mahabad dam from 2017 to 2024 using Sentinel-1 imagery with VV polarization.

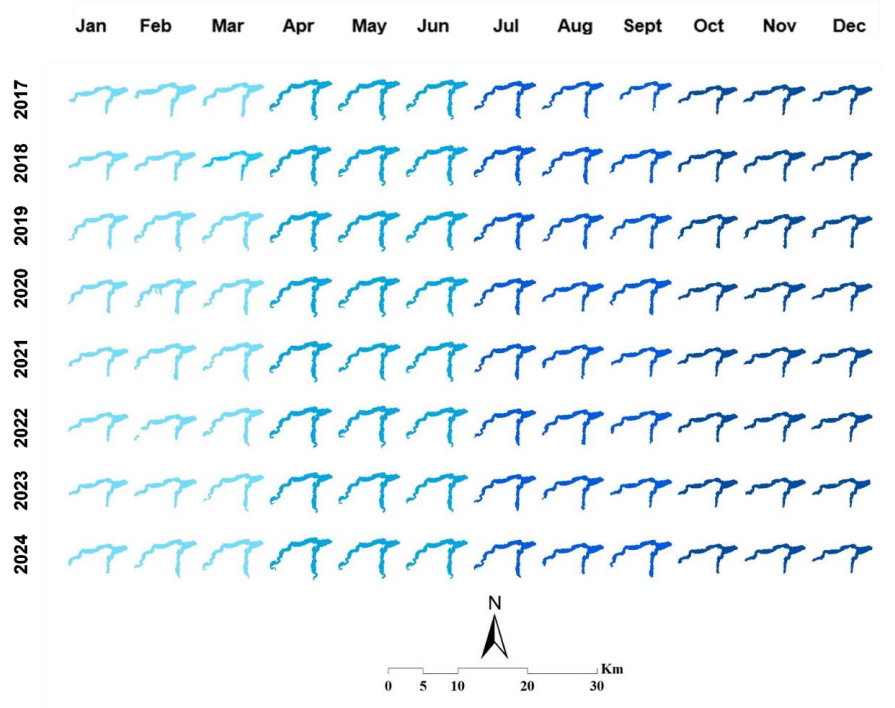

Figure 4. Changes in the water surface area of Mahabad dam from 2017 to 2024 using Sentinel-1 imagery with VH polarization.

Table 3. Seasonal averages of precipitation, humidity, temperature, and evaporation (2017–2024)

Year	Season	Precipitation (P) (mm)	Relative Humidity (RH) (%)	Temperature (T) (°C)	Evaporation (E) (mm)
2017	Winter	4.65	73.95	2.12	0.00
	Spring	36.71	47.39	13.24	138.27
	Summer	0.37	22.02	26.38	302.80
	Autumn	23.23	38.10	15.66	142.30
2018	Winter	31.29	65.17	2.37	8.87
	Spring	47.76	52.24	13.85	83.83
	Summer	0.20	27.86	25.86	279.47
	Autumn	19.74	48.47	15.57	131.87
2019	Winter	87.96	65.90	3.64	8.87
	Spring	74.71	55.47	11.67	99.83
	Summer	0.00	28.47	25.51	273.37
	Autumn	13.40	44.34	14.83	123.63
2020	Winter	67.92	71.59	2.22	0.00
	Spring	59.42	53.75	13.13	103.97
	Summer	0.73	31.75	24.36	267.30
	Autumn	44.45	46.35	15.34	123.80
2021	Winter	39.48	74.97	1.51	2.30
	Spring	25.45	41.97	14.93	127.33
	Summer	0.83	23.68	26.37	286.63
	Autumn	16.54	42.93	15.63	145.67
2022	Winter	79.29	68.64	2.73	4.30
	Spring	32.27	49.65	12.53	110.03
	Summer	0.67	29.88	26.35	279.10
	Autumn	26.17	43.68	16.95	158.90
2023	Winter	50.08	67.50	3.96	2.83
	Spring	59.50	49.40	13.79	127.87
	Summer	0.27	32.09	26.25	297.10
	Autumn	16.17	47.75	16.84	153.23
2024	Winter	44.07	62.13	4.63	0.00
	Spring	55.07	51.88	13.24	136.03
	Summer	1.13	35.67	25.98	273.87
	Autumn	19.14	49.42	15.19	142.73

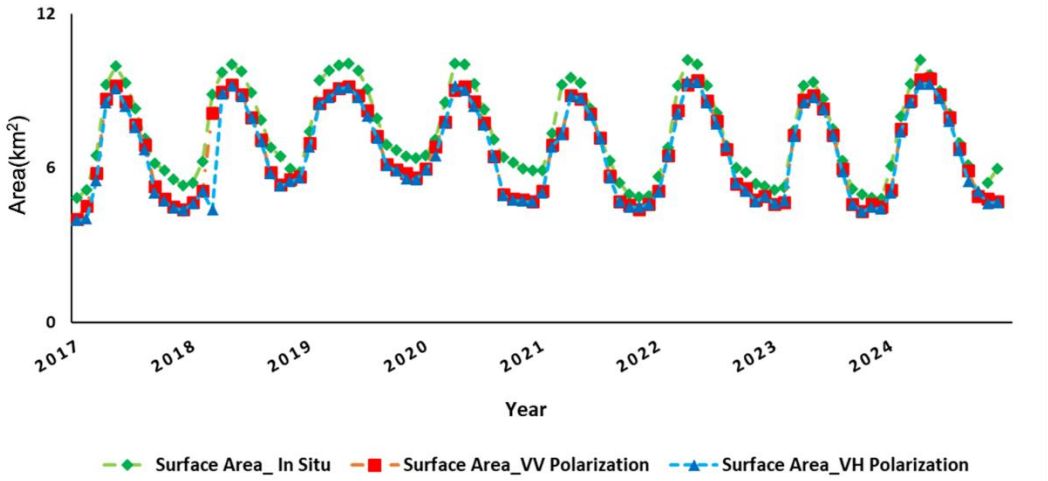

Figure 5. The time series of surface areas derived from the processing of VV and VH polarizations of Sentinel-1A SAR images, along with the local in-situ surface areas for the Mahabad dam.

The accuracy of the SVM-based water surface classification was evaluated using the multi-year mean values of Overall Accuracy (OA), Kappa coefficient, Producer Accuracy (PA), and User Accuracy (UA) over the entire study period from 2017 to 2024. The assessment was conducted separately for VV and VH polarizations, and the results are summarized using radar charts (Figure 6). This analysis provides an overall performance overview independent of short-term temporal fluctuations.

For the VV polarization, the radar diagram indicates consistently high accuracy across all metrics. OA and the Kappa coefficient exhibit values close to 1.00, reflecting strong overall classification performance and high agreement with reference data. Similarly, PA and UA show high and comparable values, indicating a balanced ability to correctly identify water pixels while minimizing omission and commission errors.

In contrast, the VH polarization shows slightly lower mean accuracy values compared to VV. Although OA and the Kappa coefficient remain high, PA and UA exhibit greater variability, suggesting a comparatively lower sensitivity of VH polarization in delineating water surfaces, particularly under complex boundary and low-water conditions. Nevertheless, the overall performance of VH polarization remains robust, with all accuracy metrics indicating reliable classification results.

Overall, the accuracy assessment based on multi-year mean values confirms that the SVM classifier performs effectively for water surface extraction using Sentinel-1 SAR data. While this analysis highlights the superior average performance of VV polarization, the temporal stability and month-to-month variability of classification accuracy are further examined in Table 4.

Table 4. Summary of classification accuracy metrics for SVM-based water surface extraction using VH and VV polarizations (2017–2024).

Polarization	Performance level	OA	Kappa	PA	UA
VH	Best month(s)	1.00	1.00	1.00	1.00
	Worst month	~0.82	~0.63	~0.66	~0.87
	Mean (2017–2024)	~0.95	~0.90	~0.93	~0.96
VV	Best month(s)	1.00	1.00	1.00	1.00
	Worst month	~0.84	~0.66	~0.65	~0.77
	Mean (2017–2024)	~0.97	~0.94	~0.96	~0.98

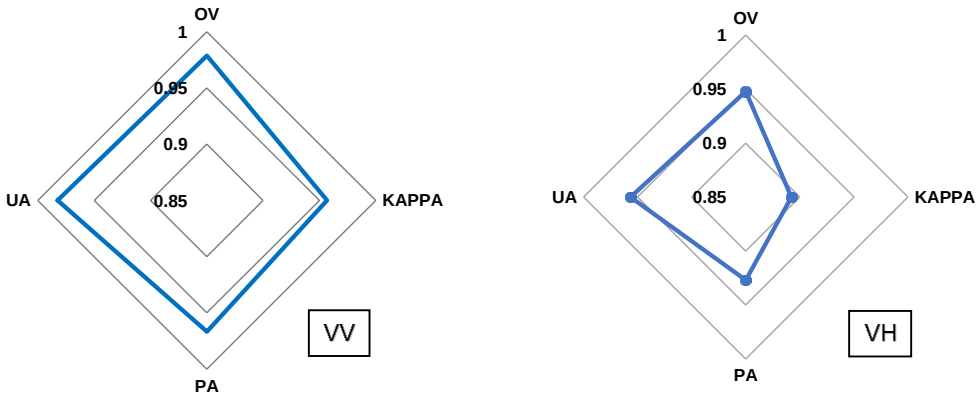

Figure 6. Accuracy assessment results for SVM classification using VV and VH polarization, including overall accuracy, kappa coefficient, producer accuracy, and user accuracy.

- **Analysis of correlation in seasons**

The seasonal correlation between water surface areas derived from Sentinel-1 SAR imagery and in-situ measurements was evaluated for VV and VH polarizations using the SVM classifier (Figure 7). The analysis indicates a very strong positive linear relationship across all seasons, with Pearson correlation coefficients of 0.99 for VV and 0.98 for VH polarization.

Seasonal patterns are clearly reflected in the scatter distribution. The largest water surface areas occur in spring due to increased precipitation and snowmelt, while the smallest extents are observed in autumn as a result of reduced rainfall and increased water withdrawal. Summer shows intermediate surface areas influenced by high evaporation rates, whereas winter exhibits greater variability, likely associated with episodic precipitation and reservoir operation changes.

The consistently high correlations across seasons confirm that the SAR-derived water surface areas effectively capture seasonal variability, with the VV polarization showing slightly stronger agreement with in-situ observations.

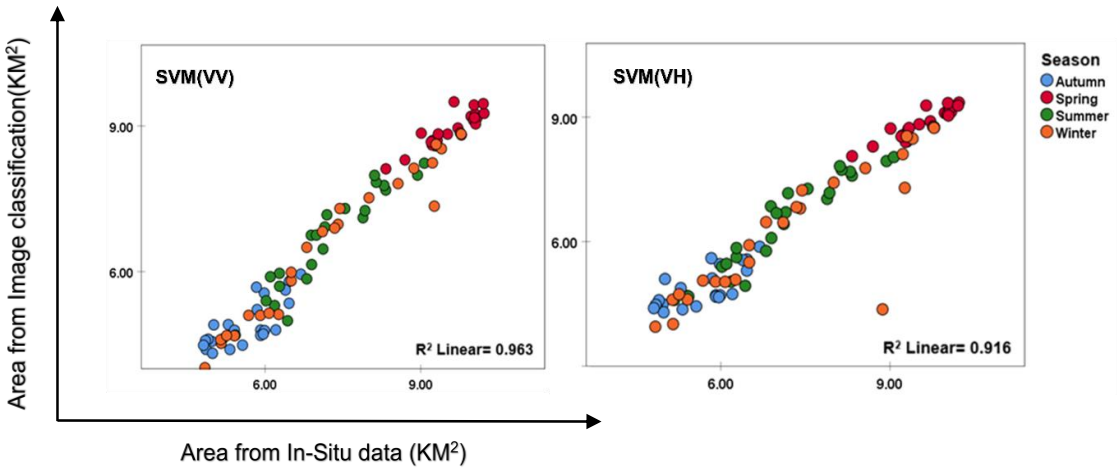

Figure 7. Seasonal correlation of areas extracted from VV and VH.

- **Result of water surface prediction**

To evaluate the performance of the proposed model for predicting water surface area, five statistical metrics were used: RMSE, MAE, R^2, NSE, and the Willmott Index (WI). Lower RMSE and MAE values represent smaller prediction errors, while higher R^2, NSE, and WI indicate stronger agreement between predicted and observed values. Ten scenarios were developed using different combinations of

SVM-derived water surface information and climatic variables, including evaporation (E), precipitation (P), temperature (T), and relative humidity (RH). The statistical performance of all scenarios on the training dataset is summarized in Table 5.

The testing results show that the model performs well across most scenarios, with R^2 values ranging from 0.848 to 0.911 and WI between 0.955 and 0.977. Among all scenarios, Scenario 3 (SVM + E) achieved the best performance, with the lowest RMSE (0.526) and MAE (0.464), and the highest R^2, NSE (0.911), and WI (0.977). The results show thaevaporation is the most influential climatic factor for predicting water surface variations. Scenario 1 (SVM + T), Scenario 5 (SVM + E + T), and Scenario 6 (SVM + E + RH) also produced strong results, while Scenario 4 (SVM + P) showed the weakest performance, indicating that precipitation alone is insufficient for accurate prediction. Scenarios involving multiple variables provided stable but not superior results compared to simpler combinations.

Figure 8 shows the distribution of predicted values across all scenarios, highlighting the superior performance of Scenario 3, which exhibits the closest alignment with observed values and the lowest dispersion. Scenarios 1, 5, and 6 also demonstrate good accuracy, while Scenario 4 appears as the least reliable. Figure 9 compares the distributions of predicted and observed water surface areas. Scenarios involving evaporation show almost identical mean (μ) and standard deviation (σ) values between predicted and observed data, indicating that the model effectively captures both the central tendency and variability of surface water dynamics. Slight deviations in σ for weaker scenarios reflect a reduced ability to represent extreme fluctuations. Overall, Figures 8, 9 and 10 confirm the robustness of the proposed approach and emphasize the significant role of evaporation in improving water surface area prediction.

Table 5. Statistical performance of different methods on the training dataset in the XGBoost model.

Testing	Statistical parameters				
	RMSE	MAE	R^2	NSE	WI
Scenario 1	0.542	0.47	0.905	0.905	0.976
Scenario 2	0.633	0.553	0.871	0.871	0.967
Scenario 3	0.526	0.464	0.911	0.911	0.977
Scenario 4	0.686	0.598	0.848	0.848	0.955
Scenario 5	0.574	0.504	0.894	0.894	0.973
Scenario 6	0.578	0.499	0.892	0.892	0.972
Scenario 7	0.608	0.545	0.881	0.881	0.967
Scenario 8	0.609	0.539	0.881	0.881	0.968
Scenario 9	0.628	0.548	0.873	0.873	0.965
Scenario 10	0.613	0.535	0.879	0.879	0.967

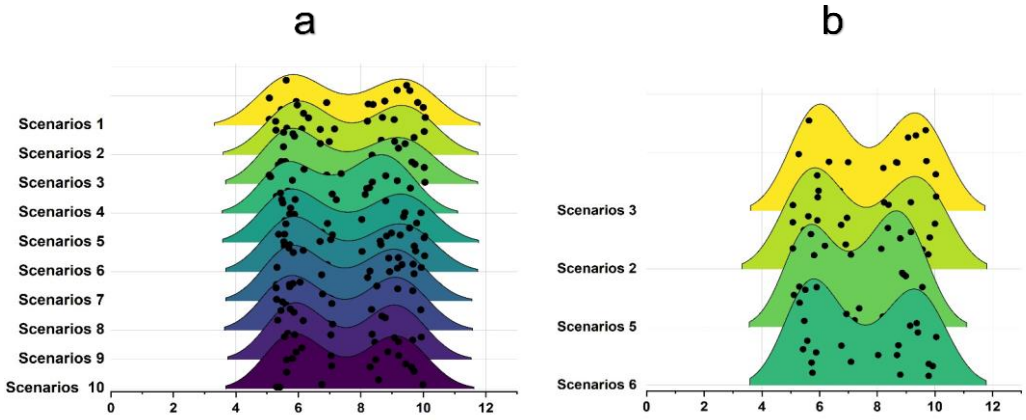

Figure 8. Distribution of predicted reservoir surface area across different modeling scenarios during the study period: (a) all evaluated scenarios and (b) top-performing scenarios.

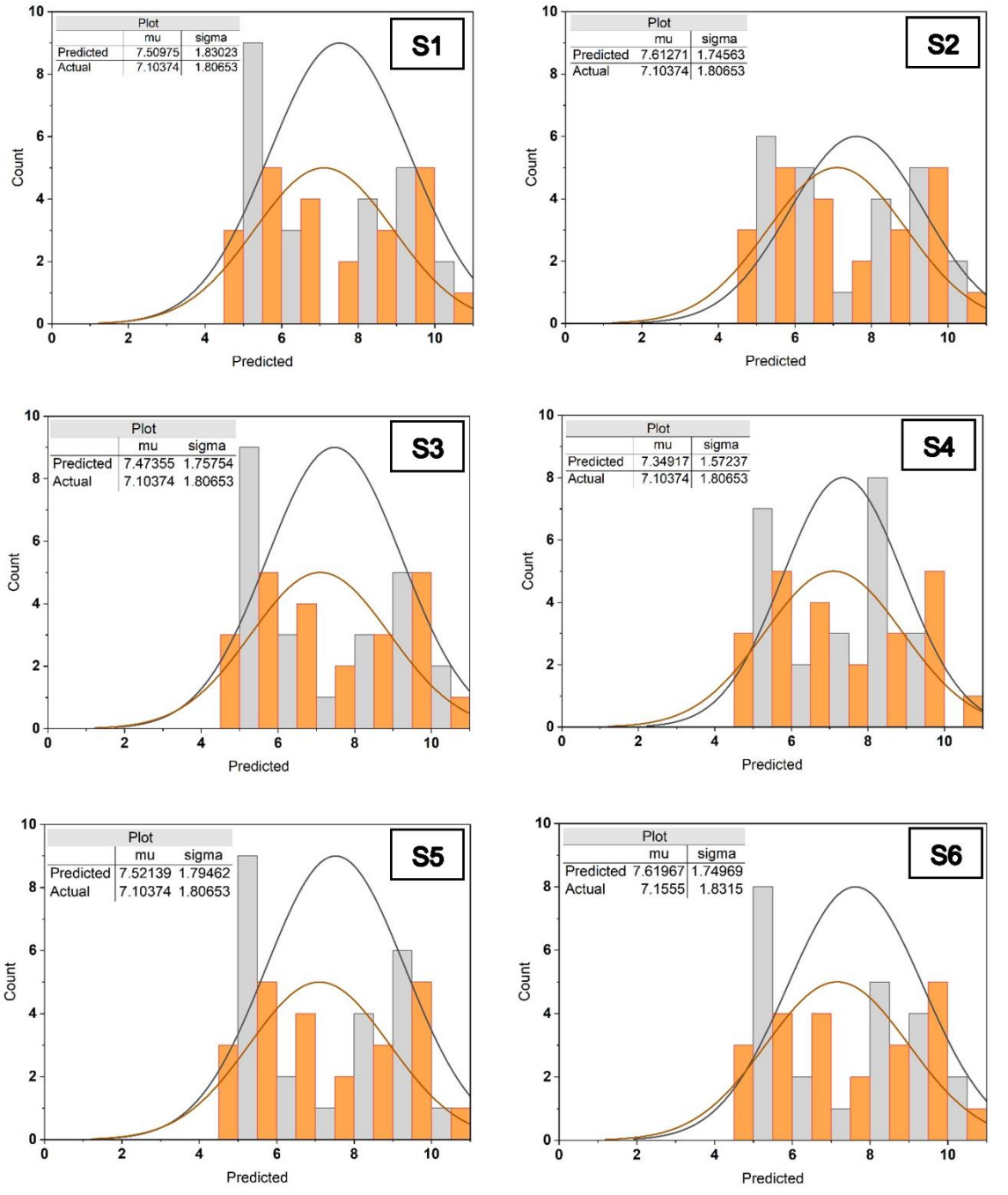

Figure 9. Histogram plots indicating the frequency of actual and predicted Area.

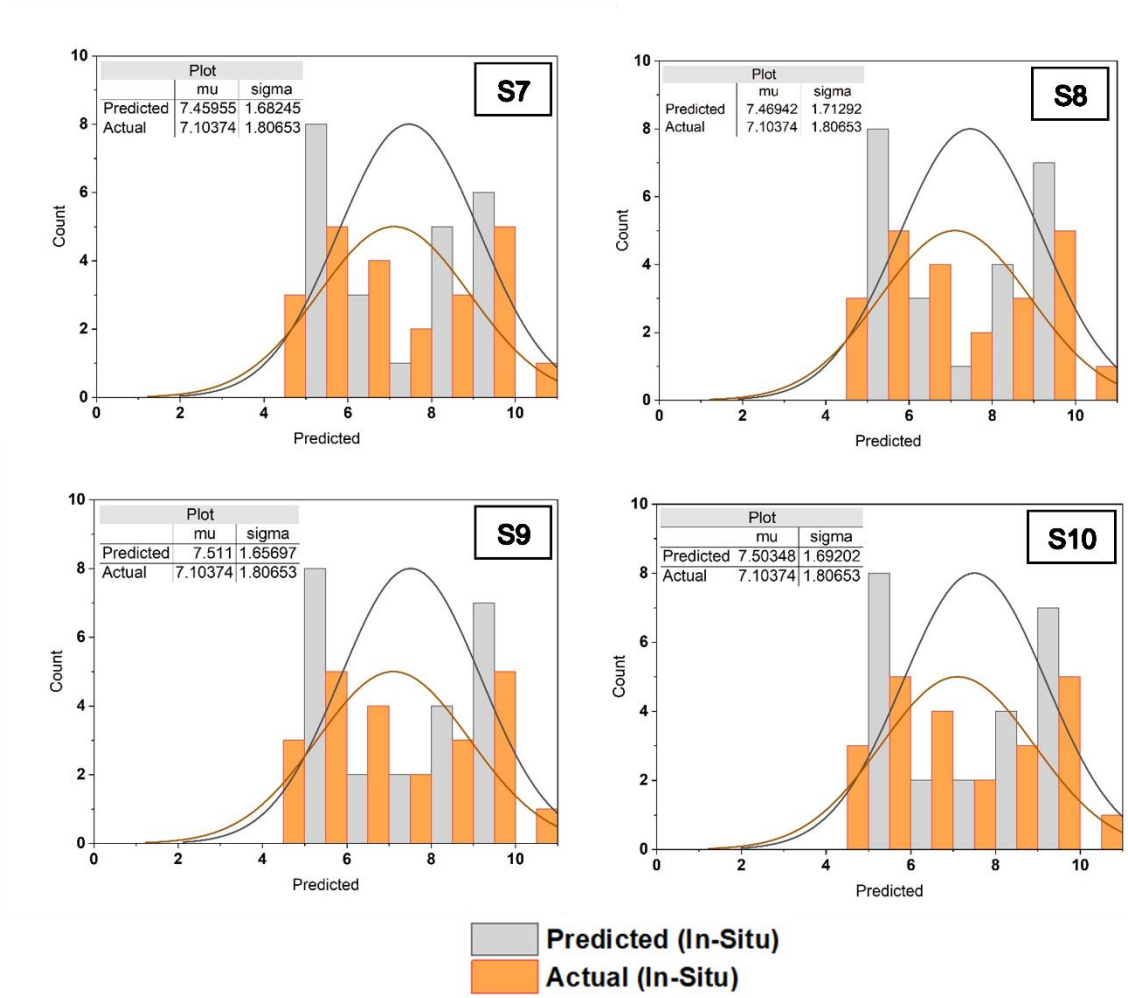

Figure 10. Histogram plots indicating the frequency of actual and predicted Area(continued).

Discussion

The results demonstrate that the proposed modeling framework can reliably predict surface water area by integrating SVM-derived water surface information with selected climatic variables. The consistently low RMSE and MAE values, together with high R^2, NSE, and WI across most scenarios, indicate strong agreement between simulated and observed water surface dynamics. These performance levels are comparable to, and in several cases exceed, those reported in previous remote sensing–based reservoir monitoring studies using machine learning approaches, particularly in semi-arid environments, confirming the competitiveness of the proposed framework. Among the evaluated scenarios, those incorporating evaporation (E) consistently achieved superior performance, with Scenario 3 (SVM + E) yielding the lowest prediction errors and highest agreement with observations. This result is hydrologically meaningful, as evaporation represents a dominant water loss mechanism in semi-arid regions and directly controls short-term fluctuations in reservoir surface area. In contrast, the relatively weak performance of Scenario 4 (SVM + P) suggests that precipitation alone cannot adequately explain surface water variations. This behavior can be attributed to hydrological delays, catchment buffering, and storage effects within the reservoir, whereby rainfall impacts are temporally lagged and modulated by inflow routing and operational controls rather than producing an immediate surface response. Interestingly, scenarios combining multiple climatic variables did not always outperform simpler configurations. This indicates that increasing input dimensionality does not necessarily enhance predictive skill and may introduce redundancy or noise, especially when correlated variables are included. The strong performance of parsimonious scenarios highlights the

importance of careful input selection over model complexity and demonstrates the efficiency of the proposed framework in extracting the most informative signals from both remote sensing and climatic data. Despite these strengths, several sources of uncertainty should be acknowledged. These include potential errors in SAR-based water surface extraction, temporal mismatches between satellite observations and climatic records, and the assumption of stationarity in the modeled relationships. Additionally, reservoir management practices and unobserved inflow dynamics were not explicitly incorporated, which may influence surface water variability. Future research could address these limitations by incorporating time-lagged climatic variables, inflow and discharge data, and reservoir operation records to better capture hydrological memory effects. The use of ensemble or hybrid modeling approaches, as well as uncertainty quantification frameworks, may further improve robustness. Extending the methodology to multiple reservoirs and climatic settings would also support broader generalization of the proposed approach.

Conclusion

This study presents an effective framework for predicting surface water area by integrating SVM-derived water surface information with climatic variables. The proposed model demonstrated strong predictive performance across ten evaluated scenarios, achieving low prediction errors and high agreement between predicted and observed water surface areas during the testing phase. Overall, RMSE values ranged from 0.526 to 0.686, while the coefficient of determination (R^2) varied between 0.848 and 0.911, confirming the robustness and reliability of the modeling approach. Among the evaluated scenarios, Scenario 3 exhibited the best performance (RMSE = 0.526, MAE = 0.464, R^2 = 0.911, NSE = 0.911, WI = 0.977), highlighting evaporation as the most influential climatic variable for improving prediction accuracy. In contrast, Scenario 4, which relied primarily on precipitation, showed the weakest performance (RMSE = 0.686, R^2 = 0.848), indicating that precipitation alone has limited explanatory power for surface water variations. This behavior can be attributed to hydrological delays and storage effects within the reservoir system, which decouple short-term rainfall from immediate changes in surface water area.

The results further demonstrate that simpler input configurations can achieve accuracy comparable to, or even better than, more complex multi-variable scenarios. Scenarios with limited but physically meaningful inputs consistently performed well, emphasizing that careful input selection is more critical than increasing model complexity. Overall, the proposed framework provides a reliable and practical tool for monitoring and predicting surface water dynamics using remote sensing and climatic data. This approach can effectively support water resource management, reservoir monitoring, and drought assessment, particularly in data-scarce regions. Future research should focus on extending the analysis to longer time series, incorporating extreme hydrological events, and integrating additional remote sensing products to further enhance model generalization and predictive capability.

References

Ahmad, S.K., Hossain, F., Eldardiry, H. and Pavelsky, T.M., (2019). A fusion approach for water area classification using visible, near infrared and synthetic aperture radar for South Asian conditions. *IEEE Transactions on Geoscience and Remote Sensing*, 58(4), pp.2471-2480.

Asghari Saraskanroud, S. , khonkham, S. and abdi, O. (2024). Evaluation of water indicators using Landsat and Sentinel satellite images (case area: Zaribar Lake). *Remote Sensing and GIS Applications in Environmental Sciences*, 4(12), 115-95. doi: 10.22034/rsgi.2024.64194.1111[in Persian].

Bagheri, S., Karimzadeh, S., Feizizadeh, B., & Samadianfard, S. (2025). *An integrated data-driven approach using dual polarized SAR data for spatiotemporal analysis of water surface changes*. Advances in Space Research. Advance online publication.

Bao, L., Lv, X. and Yao, J., 2021. Water extraction in SAR images using features analysis and dual-threshold graph cut model. *Remote Sensing*, 13(17), p.3465.https://doi.org/10.3390/rs13173465

Bolanos, S., Stiff, D., Brisco, B. and Pietroniro, A., 2016. Operational surface water detection and monitoring using Radarsat 2. Remote Sensing, 8(4), p.285.

Brisco, B., (2015). *Mapping and monitoring surface water and wetlands with synthetic aperture radar*. Remote Sensing of Wetlands: Applications and Advances, pp.119-136.

Cohen, J., (1960). A coefficient of agreement for nominal scales. *Educational and psychological measurement*, 20(1), pp.37-46.

Congalton, R.G. and Green, K., (2019). *Assessing the accuracy of remotely sensed data: principles and practices*. CRC press.

Crétaux, J.F., Abarca-del-Río, R., Berge-Nguyen, M., Arsen, A., Drolon, V., Clos, G. and Maisongrande, P., 2016. Lake volume monitoring from space. *Surveys in Geophysics*, 37(2), pp.269-305.

Foody, G.M. and Mathur, A., 2004. A relative evaluation of multiclass image classification by support vector machines. *IEEE Transactions on geoscience and remote sensing*, 42(6), pp.1335-1343.

Goumehei, E., Tolpekin, V., Stein, A. and Yan, W., 2019. Surface water body detection in polarimetric SAR data using contextual complex Wishart classification. *Water Resources Research*, 55(8), pp.7047-7059.

Guo, Z., Wu, L., Huang, Y., Guo, Z., Zhao, J. and Li, N., 2022. Water-body segmentation for SAR images: past, current, and future. *Remote Sensing*, 14(7), p.1752.

Hong, S., Jang, H., Kim, N. and Sohn, H.G., 2015. Water area extraction using RADARSAT SAR imagery combined with landsat imagery and terrain information. *Sensors*, 15(3), pp.6652-6667.

Karimzadeh, S. , Ali Azeez, A. , Valizadeh Kamran, K. and Matsuoka, M. (2025). Surface subsidence over a large structure using SBAS-InSAR with ALOS-2 PALSAR-2 data: The case of Mosul Dam, Iraq. *Remote Sensing and GIS Applications in Environmental Sciences*, 5(15), 71-47. doi: 10.22034/rsgi.2025.65859.1120

Kreiser, Z., Killough, B. and Rizvi, S.R., (2018, July). *Water across synthetic aperture radar data (wasard): Sar water body classification for the open data cube*. In IGARSS 2018-2018 IEEE International Geoscience and Remote Sensing Symposium (pp. 437-440). IEEE.

Li, J. and Wang, S., 2015. An automatic method for mapping inland surface waterbodies with Radarsat-2 imagery. *International Journal of Remote Sensing*, 36(5), pp.1367-1384.

Li, M., Hong, L., Guo, J. and Zhu, A., (2022). Automated extraction of lake water bodies in complex geographical environments by fusing Sentinel-1/2 Data. *Water*, 14(1), p.30.

Liang, J. and Liu, D., 2020. A local thresholding approach to flood water delineation using Sentinel-1 SAR imagery. *ISPRS journal of photogrammetry and remote sensing*, 159, pp.53-62.

Lv, W., Yu, Q. and Yu, W., (2010, October). *Water extraction in SAR images using GLCM and support vector machine*. In IEEE 10th international conference on signal processing proceedings.

Matgen, P., Hostache, R., Schumann, G., Pfister, L., Hoffmann, L. and Savenije, H.H.G., (2011). ***Towards an automated SAR-based flood monitoring system: Lessons learned from two case studies***. *Physics and Chemistry of the Earth*, Parts A/B/C, 36(7-8), pp.241-252.

McFeeters, S.K., 1996. The use of the Normalized Difference Water Index (NDWI) in the delineation of open water features. *International journal of remote sensing*, 17(7), pp.1425-1432.

Medina, C.E., Gomez-Enri, J., Alonso, J.J. and Villares, P., 2008. Water level fluctuations derived from ENVISAT Radar Altimeter (RA-2) and in-situ measurements in a subtropical waterbody: Lake Izabal (Guatemala). *Remote Sensing of Environment*, 112(9), pp.3604-3617.

Morandeira, N.S., Grings, F., Facchinetti, C. and Kandus, P., 2016. Mapping plant functional types in floodplain wetlands: an analysis of C-band polarimetric SAR data from RADARSAT-2. *Remote Sensing*, 8(3), p.174.

Mountrakis, G., Im, J. and Ogole, C., 2011. Support vector machines in remote sensing: A review. *ISPRS journal of photogrammetry and remote sensing*, 66(3), pp.247-259.

Noroozi Moghadam, F. , Soleimani Moghadam, H. and Akbari, E. (2025). Investigating the effective geographic factors on the subsidence of Mashhad using the model ols. *Remote Sensing and GIS Applications in Environmental Sciences*, 5(14), 37-21. doi: 10.22034/rsgi.2025.63505.1099[in Persian].

Qin, X., Yang, J., Li, P. and Sun, W., (2019, July). *Research on water body extraction from Gaofen-3 imagery based on polarimetric decomposition and machine learning*. In IGARSS 2019-2019 IEEE International Geoscience and Remote Sensing Symposium (pp. 6903-6906). IEEE.

Rajendiran, N. and Kumar, L.S., (2023). Pixel level feature extraction and machine learning classification for water body extraction. *Arabian Journal for Science and Engineering*, 48(8), pp.9905-9928.

Santoro, M., Wegmüller, U., Lamarche, C., Bontemps, S., Defourny, P. and Arino, O., 2015. Strengths and weaknesses of multi-year Envisat ASAR backscatter measurements to map permanent open water bodies at global scale. *Remote Sensing of Environment*, 171, pp.185-201.

Schölkopf, B. and Smola, A.J., (2002). *Learning with kernels: support vector machines, regularization, optimization, and beyond*. MIT press.

Stehman, S.V., (1997). Selecting and interpreting measures of thematic classification accuracy. *Remote sensing of Environment*, 62(1), pp.77-89.

Weekley, D. and Li, X., 2019. Tracking multidecadal lake water dynamics with Landsat imagery and topography/bathymetry. *Water Resources Research*, 55(11), pp.8350-8367.

Wu, L., Wang, L., Min, L., Hou, W., Guo, Z., Zhao, J. and Li, N.,(2018). Discrimination of algal-bloom using spaceborne SAR observations of Great Lakes in China. *Remote Sensing*, 10(5), p.767.

Xu, H., 2006. Modification of normalised difference water index (NDWI) to enhance open water features in remotely sensed imagery. *International journal of remote sensing*, 27(14), pp.3025-3033.

Yang, S., Wang, L., Yuan, Y., Fan, L., Wu, Y., Sun, W. and Yang, G., (2024). *Recognition of small water bodies under complex terrain based on SAR and optical image fusion algorithm*. Science of The Total Environment, 946, p.174329.

Zhang, P., Chen, L., Li, Z., Xing, J., Xing, X. and Yuan, Z., (2019). Automatic extraction of water and shadow from SAR images based on a multi-resolution dense encoder and decoder network. *Sensors*, 19(16), p.3576.

Zhou, Y.N., Luo, J., Shen, Z., Hu, X. and Yang, H., 2014. Multiscale water body extraction in urban environments from satellite images. *IEEE Journal of selected topics in applied earth observations and remote sensing*, 7(10), pp.4301-4312.